



From discrete element simulations to a continuum model

S. Luding^{a,*}, M. Lätzel^a, W. Volk^b, S. Diebels^b, H.J. Herrmann^a

^a *Institute for Computer Applications 1, Pfaffenwaldring 27, 70569 Stuttgart, Germany*

^b *Institute of Applied Mechanics (Civil Engrg.), Pfaffenwaldring 7, 70569 Stuttgart, Germany*

Received 2 November 2000; received in revised form 7 December 2000

Abstract

One of the essential questions in material sciences and especially in the area of granular matter is, how to obtain macroscopic quantities like velocity-field, stress or strain from “microscopic” quantities like contact-forces and deformations as well as particle-displacements and rotations in a granular assembly. We examine a two-dimensional (2D) shear-cell by means of discrete element simulations and compute kinematic quantities like the velocity field, the elastic deformation gradient and the deformation rate. Furthermore, we examine the density, the coordination number, the fabric and the stress. From some combinations of those quantities, one gets, e.g., the bulk-stiffness of the granulate and its shear modulus. The bulk modulus is a linear function of the trace of the fabric tensor which itself is proportional to the density and the coordination number. Finally, we note that the fabric, the stress and the strain tensors are *not co-linear* so that a more refined analysis than classical isotropic elasticity theory is required here. Another result is that the displacement rate (velocity) in the shear zone decays exponentially with the distance from the moving wall which applies the shear. Connected to the shear deformation is a rotation of the innermost layers in opposite direction, i.e., these layers roll over each other. © 2001 Elsevier Science B.V. All rights reserved.

Keywords: Micro–macro description; Couette shear cell; Fabric tensor; Stress- and strain-averaging; Shear bands; DEM simulations anisotropic materials

1. Introduction

Macroscopic continuum equations for the description of the behavior of granular media rely on constitutive equations, functions of stress, strain, and other physical quantities describing the state of the system. One possible way of obtaining an observable like the stress is to perform experiments in a two-dimensional (2D) geometry with photo-elastic material, where stress is visualized via crossed polarizers [1,2]. The alternative is, to perform discrete particle simulations [3,4] and to average over the “microscopic” quantities in the simulation, in order to obtain averaged macroscopic quantities. Besides the trivial definitions for averages over scalar quantities like density, velocity and spin, one can find in the literature, slightly different definitions for stress and strain averaging procedures [5–11].

In the following, we will briefly introduce the boundary conditions for our model system, before presenting the averaging procedure applied here. Due to the cylindrical symmetry of the problem, the corresponding continuous relations can be reduced to a simpler form, as shown below. Kinematic and dynamic quantities of the system are obtained from the simulation data and some material properties are determined as combinations of the observables.

* Corresponding author. Tel.: +711-685-3593; fax: 711-685-3658.

E-mail address: lui@ica1.uni-stuttgart.de (S. Luding).

2. Model and averaging strategy

In the simulations presented in this study, a 2D Couette shear-cell is used, filled with a bidisperse packing of disks, as sketched in Fig. 1. The system is slowly sheared by turning the inner ring counter-clockwise about once per minute.

The inner ring has a radius of $R_i = 0.1032$ m and the system extends over $R_o - R_i = 0.1492$ m in radial direction. In the experiment, the height of the system is $h = 0.006$ m and it is filled with slightly less high disks of different diameters $d_s = 7.42$ mm and $d_l = 8.99$ mm, to avoid crystallization. In this study we mainly present results from one long simulation with $N = N_s + N_l$ particles, with $N_s = 2538$ and $N_l = 407$. The angular frequency of the inner ring is $\Omega = 2\pi/T = 0.1$ s⁻¹ and the simulation is performed until $t = 500$ s; for the averaging, we disregard the first two rotations. For more details see [10,11].

The averaging procedure, as applied in the following, can be formalized for any quantity Q , keeping in mind that we first average over each particle and then attribute a fraction of each particle – and thus a fraction of Q – to the corresponding averaging volume. An alternative approach, i.e., to use the fraction of the center-center line of the particles instead of the volume [12], is not applied here. In equations, our ansatz reads

$$Q = \langle Q^p \rangle = \frac{1}{V} \sum_{p \in V} w_V^p V^p Q^p, \quad (1)$$

with the pre-averaged particle quantity $Q^p = \sum_{c=1}^{C^p} Q^c$ and the quantity Q^c attributed to contact c of particle p , where C^p is the number of contacts of particle p . The factor w_V^p is the weight corresponding to the fraction of the particle volume V^p which lies inside the averaging volume V . Due to the symmetry of the system, rings at radial distance r from the center and width Δr can be used, so that $V = 2\pi hr \Delta r$.

The first important quantity to measure is the volume fraction

$$v = v(r) = \frac{1}{V} \sum_{p \in V} w_V^p V^p, \quad (2)$$

obtained by using $Q^p = 1$ and disregarding the sum over the contacts. v is related to the mass density via $\rho(r) = \rho^p v$, with the material's density $\rho^p = 1060$ kg m⁻³, paralleling the experiments [1,2,10,11]. The next quantity of interest is the mean particle flux

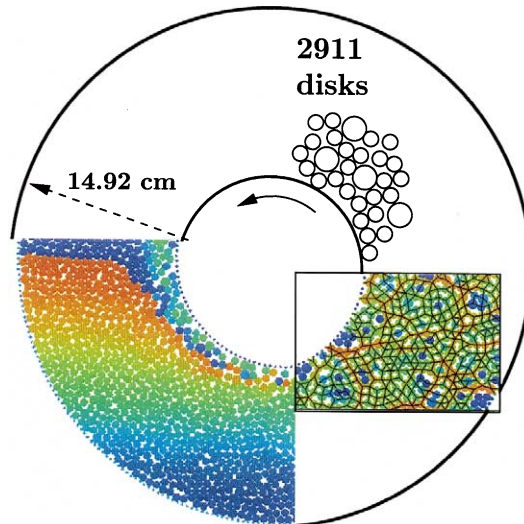


Fig. 1. Sketch of the model system. The left color inset shows the shear zone after one half rotation – particles with the same vertical coordinate had the same color initially. The right color inset shows the stress chains, where large, medium and small contact-forces are colored red, green and blue, respectively.

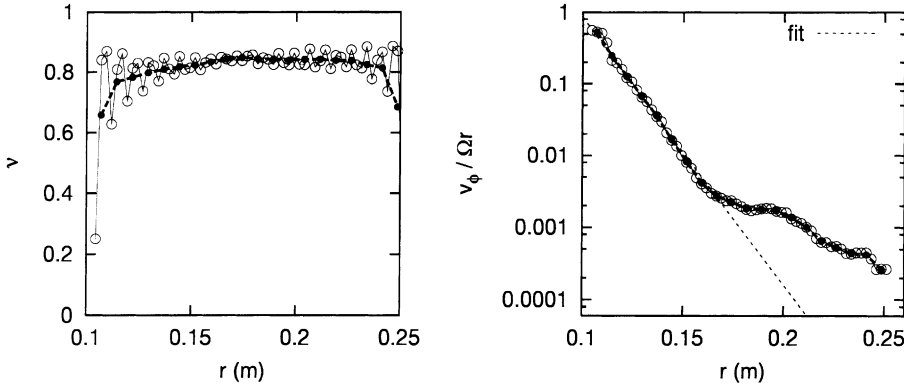


Fig. 2. Density ν and scaled velocity $v_\phi/\Omega r$, with the angular velocity Ωr of a solid body rotating with the inner ring, plotted against the distance from the center r . The closed (open) symbols correspond to 20 (60) binning intervals. The dotted line is the best fit to the velocity in the shear zone $v_\phi(r) = v_0 \exp(-(r - R_i)/s)$, with $v_0/(\Omega R_i) = 0.645$ and $s = 0.0127$ m.

$$\nu v_\phi = \frac{1}{V} \sum_{p \in V} w_V^p V^p v_\phi^p \quad (3)$$

obtained with $\underline{Q}^p = v_\phi^p$, the tangential velocity of particle p . We checked that $v_r \approx 0$ in accordance with the assumption of a steady-state shear situation. In Fig. 2, the density and the velocity are plotted against the distance from the center r . We identify the shear zone with those parts of the system with sufficiently large v_ϕ . Like in the experiments, the material is dilated in the shear-zone near the inner, rotating wall and also in the vicinity of the outer boundary, whereas it is densified in the central part (due to mass conservation and the fixed volume boundary conditions). Particles are layered close to the walls, as indicated by the periodic wiggles in high-resolution density, but no order effects are visible in the inner parts of the system. The velocity decays exponentially from the inner ring over two orders of magnitude, before it reaches some noise-level; the fit (dotted line) is performed in the range of decay.

3. Fabric, stress and elastic strain

The fabric tensor, in our definition, involves the so-called branch vectors $\mathbf{l}^{pc} = (d^p/2)\mathbf{n}^c$ from the center of particle p with diameter d^p to its contact c , with the contact normal vector \mathbf{n}^c , so that

$$\mathbf{F} = \langle \mathbf{F}^p \rangle = \frac{1}{V} \sum_{p \in V} w_V^p V^p \sum_{c=1}^{C^p} \mathbf{n}^c \otimes \mathbf{n}^c, \quad (4)$$

when using $V^p = \pi h (d^p/2)^2$, the volume of a disk. The tensor \mathbf{F} is normalized so that its trace $\text{tr}(\mathbf{F}) = \nu C$, with the mean coordination number C , for monodisperse particles. For polydisperse size distribution functions, a multiplicative correction factor was recently proposed [13]. The deviator of the fabric is a measure for the anisotropy of the contact network [10,11], see Fig. 3. In our situation, the anisotropy, i.e., the deviatoric fraction remains below 20%. The static component of the stress tensor [7,10] is defined as the dyadic product of the force \mathbf{f}^c acting at contact c with the corresponding branch vector

$$\boldsymbol{\sigma} = \langle \boldsymbol{\sigma}^p \rangle = \frac{1}{V} \sum_{p \in V} w_V^p V^p \sum_{c=1}^{C^p} \mathbf{f}^c \otimes \mathbf{l}^{pc}, \quad (5)$$

and the dynamic component of the stress tensor

$${}^d \boldsymbol{\sigma} = \langle {}^d \boldsymbol{\sigma}^p \rangle = \frac{1}{V} \sum_{p \in V} w_V^p V^p \rho^p \mathbf{v}^p \otimes \mathbf{v}^p \quad (6)$$

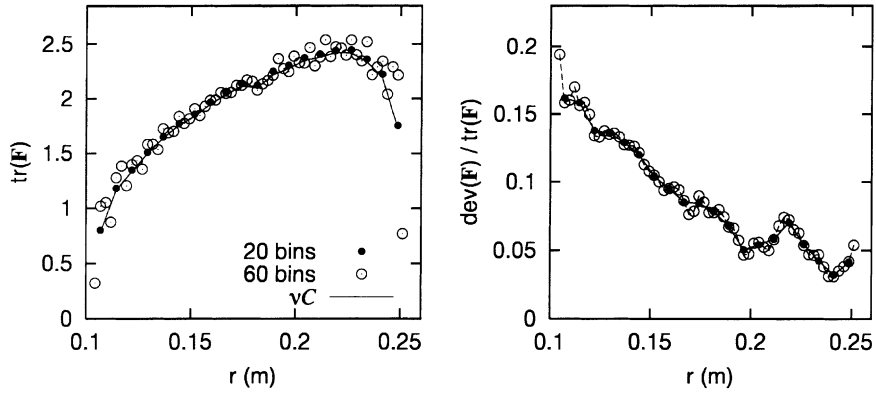


Fig. 3. Components of the fabric tensor $\text{tr}(\mathbf{F})$ (isotropic) and $\text{dev}(\mathbf{F})/\text{tr}(\mathbf{F})$ (anisotropic) for different numbers of binning intervals, as in Fig. 2.

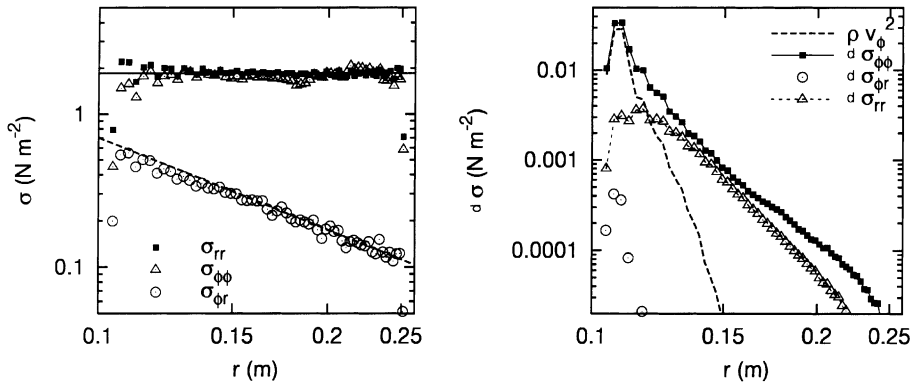


Fig. 4. Components of the static stress σ , the dynamic stress ${}^d\sigma$, and the fluctuation contribution ρv_ϕ^2 , plotted against the distance from the center r . Note the different vertical axis scaling.

has two contributions: (i) the stress due to velocity fluctuations around the mean and (ii) the stress ${}^d\sigma_{\phi\phi} \sim \rho v_\phi^2$ due to the mean mass transport in ϕ -direction. In Fig. 4, the static and the dynamic contributions are plotted. In our system, the diagonal elements of the static stress are almost constant, whereas the off-diagonal elements decay proportional to r^{-2} , as indicated by the lines. From the dynamic stress tensor, one obtains ${}^d\sigma_{\phi\phi} > {}^d\sigma_{rr} > {}^d\sigma_{\phi r}$; the velocity fluctuations lead to a small stress in all components, decreasing with increasing r . The angular velocity in the shear zone strongly contributes to ${}^d\sigma_{\phi\phi}$, however, the dynamic stress is always much smaller than the static stress, i.e., the system is quasi-static. Finally, the elastic deformation gradient [8,10,11] is defined as

$$\boldsymbol{\epsilon} = \frac{\pi h}{V} \left(\sum_{p \in V} w_V^p \sum_{c=1}^{CP} \Delta^{pc} \otimes \mathbf{l}^{pc} \right) \cdot \mathbf{A}, \quad (7)$$

where Δ^{pc} is the deformation of contact c and $\mathbf{A} = \mathbf{F}^{-1}$ is the inverse fabric tensor. The elastic deformation gradient is a measure for the mean reversible deformation of the material and thus for the energy stored in the compressed granulate. In the following, we extract some material properties from the quantities defined above.

In Fig. 5 the rescaled stiffness and some shear modulus of the granulate are plotted against the trace of the fabric. Furthermore, the orientations of the tensors, \mathbf{F} , $\boldsymbol{\sigma}$, $\boldsymbol{\epsilon}$ are plotted against the distance from the inner ring. The data for the bulk modulus from different simulations collapse on a master curve as well as the data for the shear modulus, however, the latter are strongly scattered.

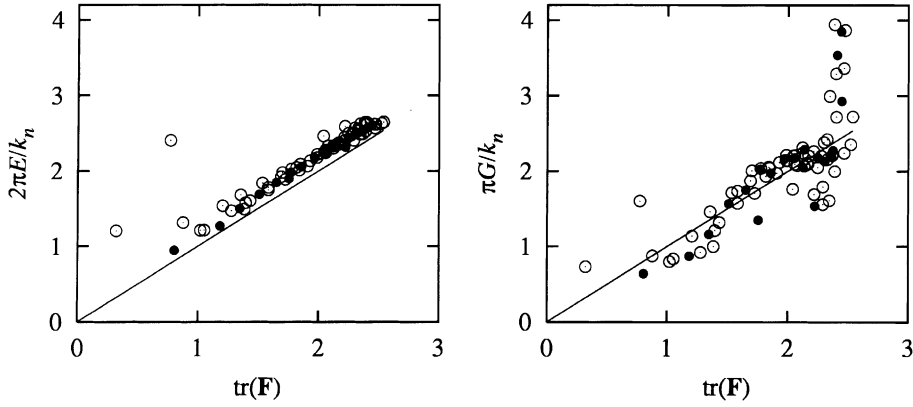


Fig. 5. Granulate stiffness $2\pi E/k_n = \text{tr}(\boldsymbol{\sigma})/\text{tr}(\boldsymbol{\epsilon})$, plotted against $\text{tr}(\mathbf{F})$. Scaled granulate shear resistance $\pi G/k_n = \text{dev}(\boldsymbol{\sigma})/\text{dev}(\boldsymbol{\epsilon})$ plotted against $\text{tr}(\mathbf{F})$, with the effective spring-constant k_n .

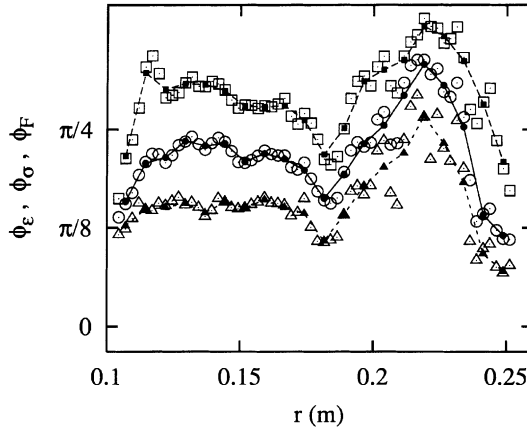


Fig. 6. Orientation of the fabric, stress, and strain-tensors (from top to bottom).

The most remarkable result in Fig. 6 is the fact that the orientations ϕ_T of the tensors are not co-linear, where ϕ_T is defined as the orientation of the “major eigenvector”, i.e., the eigenvector corresponding to the major eigenvalue of \mathbf{T} , with respect to the radial direction. Thus the averaging procedure leads to results for the fabric, the stress, and the elastic deformation gradient. The combination of some of these quantities can be interpreted as bulk- and shear-modulus, even when isotropy and co-linearity of the tensors is not the case.

4. Continuum description

Implying a steady-state situation ($\partial/\partial t = 0$) and using the cylindrical geometry of the shear cell ($\partial/\partial \phi = 0$), we obtain for the divergence of the stress tensor [14] in the 2D system

$$\nabla \cdot \boldsymbol{\sigma} = \left[\frac{1}{r} \frac{\partial(r\sigma_{rr})}{\partial r} - \frac{1}{r} \sigma_{\phi\phi} \right] \mathbf{e}_r + \left[\frac{1}{r} \frac{\partial(r\sigma_{r\phi})}{\partial r} + \frac{1}{r} \sigma_{\phi r} \right] \mathbf{e}_\phi, \quad (8)$$

with the unit vectors \mathbf{e}_r and \mathbf{e}_ϕ in radial outwards and in tangential direction, respectively. The indices r and ϕ denote the corresponding components of $\boldsymbol{\sigma}$. In static equilibrium, both components should vanish independently of each other, so that one has

$$\frac{\partial(r\sigma_{rr})}{\partial r} = \sigma_{\phi\phi} \quad \text{and} \quad \frac{\partial(r\sigma_{r\phi})}{\partial r} = -\sigma_{\phi r}. \quad (9)$$

If the diagonal and the off-diagonal elements of σ are pair-wise equal and depend on r in the same way, respectively, the above equations lead to

$$\sigma_{rr} \propto \sigma_{\phi\phi} \propto r^0 \quad \text{and} \quad \sigma_{r\phi} \propto \sigma_{\phi r} \propto r^{-2}, \quad (10)$$

almost consistent with the numerical data presented in Fig. 4.

Taking into account all stress components and the material time derivative of the velocity $\mathbf{a} = (d/dt)\mathbf{v} = (\partial/\partial t)\mathbf{v} + (\mathbf{v} \cdot \nabla)\mathbf{v}$ from which only v_ϕ^2/r survives in the radial component of \mathbf{a} , one gets the equations of motion from $\rho\mathbf{a} = \nabla \cdot \sigma$ componentwise

$$0 = \rho v_\phi^2 + r \frac{\partial \sigma_{rr}}{\partial r} + (\sigma_{rr} - \sigma_{\phi\phi}), \quad (11)$$

$$0 = r \frac{\partial \sigma_{r\phi}}{\partial r} + (\sigma_{r\phi} + \sigma_{\phi r}), \quad (12)$$

which are presented in a way that the right-hand side should vanish in Eqs. (11) and (12).

In Fig. 7, the two equations of motion are shown with the static stress contribution alone and also together with the dynamic contribution. The different stresses and their derivatives sum up to zero inside the system – at the boundary some large values survive, indicating still missing contributions.

In our geometry, the velocity gradient $\nabla\mathbf{v}$ has only two entries, namely

$$[\nabla\mathbf{v}]_{r\phi} = \frac{\partial v_\phi}{\partial r} \quad \text{and} \quad [\nabla\mathbf{v}]_{\phi r} = -\frac{v_\phi}{r}, \quad (13)$$

from which one can derive the deformation rate D and the continuum rotation W , respectively,

$$D_{r\phi} = \frac{1}{2} \left[\frac{\partial v_\phi}{\partial r} - \frac{v_\phi}{r} \right] \quad \text{and} \quad W_{r\phi} = \frac{1}{2} \left[\frac{\partial v_\phi}{\partial r} + \frac{v_\phi}{r} \right]. \quad (14)$$

In Fig. 8, the deformation rate and the spin are plotted as functions of r and are found to be in agreement with the analytical expression (in the shear zone)

$$D_{r\phi} = D_{\phi r} = -\frac{v_0}{2} \exp\left(-\frac{r-R_i}{s}\right) \left[\frac{1}{s} + \frac{1}{r}\right] \quad (15)$$

computed using the fit in Fig. 2. In order to obtain the spin, $(1/s + 1/r)$ has to be replaced by $(1/s - 1/r)$, as shown in Fig. 8, together with the spin of the particles, which is the combination of the continuum spin and the additional eigen-rotation $\omega^* = \omega - W_{r\phi}$ of the discrete particles [11]. The excess eigen-rotation of the particles, with respect to the continuum is presented in Fig. 9 and, as in the experiments of shear cell,

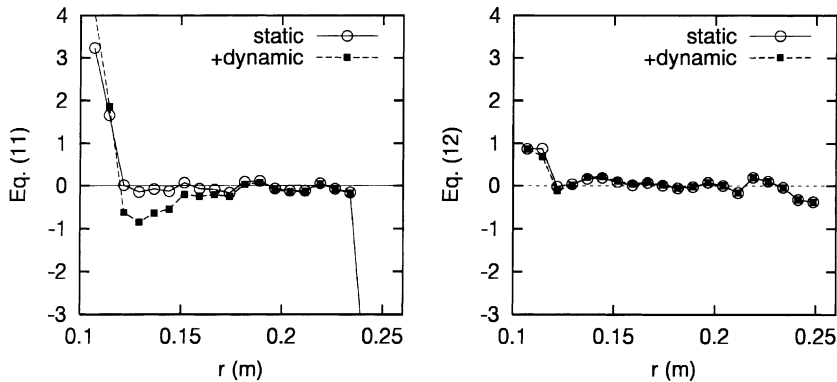


Fig. 7. Components of the equations of motion, plotted against r . The static contribution is compared to the total, including dynamic contributions.

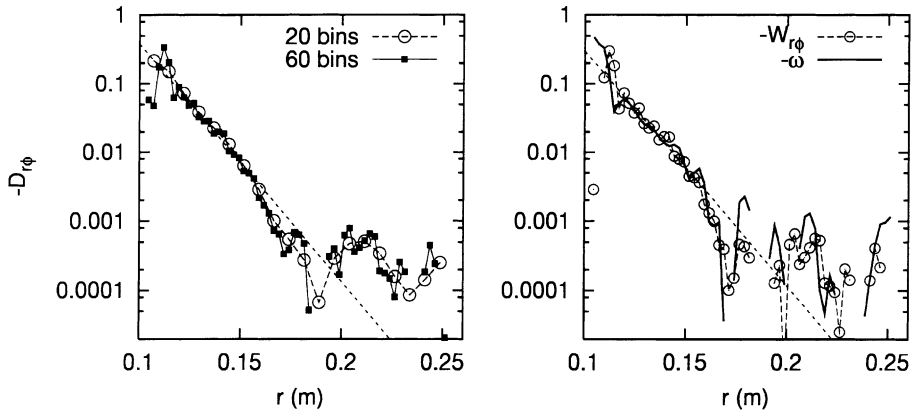


Fig. 8. Negative deformation rate and spin, plotted against r . The dotted lines are derived using the fit to v_ϕ from Fig. 2 according to Eq. (14). The solid line in the right frame gives $-\omega$, the negative mean spin of the particles.

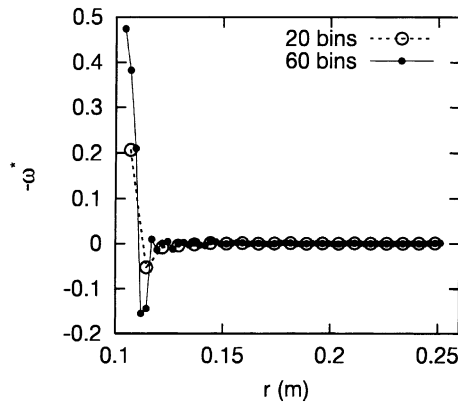


Fig. 9. Negative eigen-rotation ω^* of the particles in the shear zone, close to the inner ring. One obtains alternating rotation sense in the two innermost layers.

one obtains an alternating spin amplitude in the shear zone, indicating that the particle layers roll over each other.

5. Discussion

In summary, we used discrete element simulations and obtained kinematic and dynamic quantities in a quasi-2D ring-shear cell. In agreement with experiments, a shear-zone with exponentially decaying shear velocity is observed at the inner, moving wall. Ahead with shear goes some dilation and eigen-rotation of the discrete particles. From the data, one also obtains that the isotropic parts of fabric, stress and strain are connected via the material’s bulk modulus which is proportional to the coordination number, i.e., the trace of the fabric tensor. In a similar picture, the shear modulus shows stronger scatter, indicating additional effects not accounted for by the isotropic elastic theory implied. Due to the anisotropy, the stress-, strain- and fabric tensors are *not co-linear*. This means that even such a simple model granulate is a subtle anisotropic material which cannot be described by a classical isotropic elasticity theory and only two material parameters.

The validity of the macroscopic quantities computed here is checked by inserting the computed values into the equations of motion at different radial positions. The results presented here are rather consistent away from the boundaries and in the region of weak shear. Closer to the boundaries and in the shear-zone,

additional effects like particle rotations become important and one should use an approach involving micropolar quantities [11].

Understanding the connection between stress and strain and the influence of an anisotropic fabric is subject of current research. Furthermore, we study the influence of static friction and other microscopic material parameters on the physics of the shear-cell. In addition, the role of the shear rate and the eigen-rotation of the particles is an open issue.

Acknowledgements

We acknowledge the support of the Deutsche Forschungsgemeinschaft (DFG) and thank R.P. Behringer, W. Ehlers, D.W. Howell, D. Schaeffer, and J. Socolar for helpful discussions.

References

- [1] D.W. Howell, R.P. Behringer, Fluctuations in a 2D granular couette experiment: a critical transition, *Phys. Rev. Lett.* 82 (1999) 5241.
- [2] D.W. Howell, R.P. Behringer, C.T. Veje, Fluctuations in granular media, *Chaos, Solitons & Fractals* 9 (1999) 559.
- [3] P.A. Cundall, O.D.L. Strack, A discrete numerical model for granular assemblies, *Géotechnique* 29 (1) (1979) 47.
- [4] H.J. Herrmann, J.-P. Hovi, S. Luding (Eds.), *Physics of Dry Granular Media – NATO ASI Series E 350*, Kluwer Academic Publishers, Dordrecht, 1998.
- [5] S.B. Savage, D.J. Jeffrey, The stress tensor in a granular flow at high shear rates, *J. Fluid Mech.* 110 (1981) 225.
- [6] R.J. Bathurst, L. Rothenburg, Micromechanical aspects of isotropic granular assemblies with linear contact interactions, *J. Appl. Mech.* 55 (1988) 17.
- [7] N.P. Kruyt, L. Rothenburg, Micromechanical definition of strain tensor for granular materials, *J. Appl. Mech.* 118 (1996) 706.
- [8] C.-L. Liao, T.-P. Chang, D.-H. Young, C.S. Chang, Stress–strain relationship for granular materials based on the hypothesis of best fit, *Int. J. Solids Struct.* 34 (1997) 4087.
- [9] J.D. Goddard, Continuum modeling of granular assemblies, in: H.J. Herrmann, J.-P. Hovi, S. Luding (Eds.), *Physics of Dry Granular Media NATO ASI-E350*, Kluwer Academic Publishers, Dordrecht, 1998.
- [10] M. Lätzel, S. Luding, H.J. Herrmann, Macroscopic material properties from quasi-static microscopic simulations of a two-dimensional shear-cell, *Granular Matter* 2 (3) (2000) 123.
- [11] M. Lätzel, S. Luding, H.J. Herrmann, From discontinuous models towards a continuum description, in: P.A. Vermeer, et al. (Eds.), *Continuous and Discontinuous Modelling of Cohesive-Frictional Materials*, Springer, Berlin, 2001.
- [12] I. Goldhirsch, Note on the definition of stress for discrete systems, 1999, preprint.
- [13] M. Madadi, O. Tsoungui, M. Lätzel, S. Luding, On the fabric tensor of static, polydisperse granular materials, 2000, preprint.
- [14] L.E. Malvern, *Introduction to the Mechanics of a Continuous Medium*, Prentice-Hall, Englewood Cliffs, NJ, 1969.